DIGITAL ACCESS TO SCHOLARSHIP AT HARVARD
DASH.HARVARD.EDU

HARVARD LIBRARY
Office for Scholarly Communication

Insulator dysfunction and oncogene activation in IDH mutant gliomas

Citation
Flavahan, William A., Yotam Drier, Brian B. Liau, Shawn M. Gillespie, Andrew S. Venteicher, Anat O. Stemmer-Rachamimov, Mario L. Suvà, and Bradley E. Bernstein. 2015. "Insulator dysfunction and oncogene activation in IDH mutant gliomas." Nature 529 (7584): 110-114. doi:10.1038/nature16490. http://dx.doi.org/10.1038/nature16490.

Published Version
doi:10.1038/nature16490

Permanent link
http://nrs.harvard.edu/urn-3:HUL.InstRepos:27662216

Terms of Use
This article was downloaded from Harvard University's DASH repository, and is made available under the terms and conditions applicable to Other Posted Material, as set forth at http://nrs.harvard.edu/urn-3:HUL.InstRepos:dash.current.terms-of-use#LAA

Share Your Story

The Harvard community has made this article openly available.
Please share how this access benefits you. Submit a story .

Accessibility

Author Manuscript

Author Manuscript

Author Manuscript

Author Manuscript

HHS Public Access

Author manuscript

Nature. Author manuscript; available in PMC 2016 June 23.

Published in final edited form as:

Nature. 2016 January 7; 529(7584): 110–114. doi:10.1038/nature16490.

Insulator dysfunction and oncogene activation in IDH mutant gliomas

William A. Flavahan[1,2,3,*], **Yotam Drier**[1,2,3,*], **Brian B. Liau**[1,2,3], **Shawn M. Gillespie**[1,2,3], **Andrew S. Venteicher**[1,2,4], **Anat O. Stemmer-Rachamimov**[1], **Mario L. Suvà**[1,2], and **Bradley E. Bernstein**[1,2,3]

[1]Department of Pathology and Center for Cancer Research, Massachusetts General Hospital and Harvard Medical School, Boston, Massachusetts, USA

[2]Broad Institute of MIT and Harvard, Cambridge, Massachusetts, USA

[3]Howard Hughes Medical Institute, Chevy Chase, Maryland, USA

[4]Department of Neurosurgery, Massachusetts General Hospital and Harvard Medical School, Boston, Massachusetts, USA

Abstract

Gain-of-function *IDH* mutations are initiating events that define major clinical and prognostic classes of gliomas[1,2]. Mutant IDH protein produces a novel onco-metabolite, 2-hydroxyglutarate (2-HG), that interferes with iron-dependent hydroxylases, including the TET family of 5′-methylcytosine hydroxylases[3–7]. TET enzymes catalyze a key step in the removal of DNA methylation[8,9]. *IDH* mutant gliomas thus manifest a CpG island methylator phenotype (G-CIMP)[10,11], though the functional significance of this altered epigenetic state remains unclear. Here we show that *IDH* mutant gliomas exhibit hyper-methylation at CTCF binding sites, compromising binding of this methylation-sensitive insulator protein. Reduced CTCF binding is associated with loss of insulation between topological domains and aberrant gene activation. We specifically demonstrate that loss of CTCF at a domain boundary permits a constitutive enhancer to aberrantly interact with the receptor tyrosine kinase gene *PDGFRA*, a prominent glioma oncogene. Treatment of *IDH* mutant gliomaspheres with demethylating agent partially restores insulator function and down-regulates *PDGFRA*. Conversely, CRISPR-mediated disruption of the CTCF motif in *IDH* wildtype gliomaspheres up-regulates *PDGFRA* and increases proliferation. Our study suggests that *IDH* mutations promote gliomagenesis by disrupting chromosomal topology and allowing aberrant regulatory interactions that induce oncogene expression.

Users may view, print, copy, and download text and data-mine the content in such documents, for the purposes of academic research, subject always to the full Conditions of use: http://www.nature.com/authors/editorial_policies/license.html#terms

Correspondence should be addressed to: B.E.B. (; Email: Bernstein.Bradley@mgh.harvard.edu)

*These authors contributed equally to this work.

Conception and experimental design: W.A.F., Y.D., B.B.L., S.M.G., M.L.S., and B.E.B. Methodology and data acquisition: W.A.F., Y.D., B.B.L., S.M.G., A.S.V., A.O.S-R., M.L.S., and B.E.B. Analysis and interpretation of data: W.A.F., Y.D., and B.E.B. Manuscript writing: W.A.F., Y.D., and B.E.B. W.A.F., and Y.D. contributed equally to this report.

The authors declare no competing interests.

Data generated for this study are available through GEO accession number GSE70991.

Author Manuscript Author Manuscript Author Manuscript Author Manuscript

The human genome is organized into topological domains that represent discrete structural and regulatory units[12]. Such domains are evident in genome-wide contact maps generated by HiC[13], and have been termed 'topologically-associated domains' or 'contact domains'[14_16]. Recent studies have solidified the role of the CTCF insulator protein in creating chromatin loops and boundaries that partition such domains[15]. Genomic alterations that remove CTCF-associated boundaries allow aberrant enhancer-gene interactions and alter gene expression[17].

Since CTCF binding is methylation-sensitive[18,19], its localization might be altered by DNA hyper-methylation in *IDH* mutant gliomas. We therefore used ChIP-seq to map CTCF binding genome-wide in eleven primary tumors and four glioma lines. Although CTCF binding patterns tend to be relatively stable, we detected highly overlapping subsets of CTCF sites lost in *IDH* mutants (Fig. 1a–b; see **Methods**). Significantly more sites were commonly lost than gained (625 vs 300, $p<10^{-12}$). We used whole genome bisulfite sequencing data from the Cancer Genome Atlas (TCGA)[10] to assess the methylation status of 625 loci with reduced CTCF binding in mutant tumors. We found that these loci have higher GC content, and exhibit significantly higher levels of DNA methylation in *IDH* mutant gliomas, relative to *IDH* wildtype (Fig. 1c–d).

We considered that altered DNA methylation and CTCF binding might disrupt topological domain boundaries and gene insulation in IDH mutant tumors. We collated a set of constitutive domain boundaries based on kilobase-resolution HiC maps[15]. We then examined published RNA-seq expression data for 357 normal brain tissue samples[20]. Consistent with prior studies[16], we found that genes in the same domain correlate across samples, but that genes separated by a boundary show lower correlation (Fig. 1e). We next incorporated expression data for 230 *IDH* mutant and 56 wildtype lower-grade gliomas, generated by the Cancer Genome Atlas (TCGA)[2]. Here again we found that the presence of an intervening boundary reduces correlation between neighboring genes. We next scanned the genome for pairs of proximal genes separated by less than 180 kb (the average contact domain size[15]) that correlate much more strongly in *IDH* mutants than in wildtype gliomas (Fig. 1f; see **Methods**). Remarkably, the resulting set is strongly enriched for gene pairs that cross domain boundaries (90% vs 69% expected at random; $p<10^{-4}$). Conversely, gene pairs that correlate less strongly in *IDH* mutants are more likely to reside in the same domain (52% vs 31% expected at random; $p<10^{-5}$). Notably, CTCF knock-down has been shown to increase cross-boundary interactions and decrease intra-domain interactions[21]. Thus, altered expression patterns in *IDH* mutant gliomas may reflect reduced CTCF binding and consequent disruption of domain boundaries and topologies.

We next sought to pinpoint specific boundaries disrupted by *IDH* mutation. For all pairs of genes separated by <1 MB, we computed their correlation across *IDH* mutant gliomas and across wildtype gliomas. We then scanned for loci in which cross-boundary gene pairs correlate more strongly in mutant tumors (FDR<1%), while intra-domain gene pairs correlate less strongly (FDR<1%). This analysis highlighted 203 domain boundaries (Fig. 2a; Table S1; see **Methods**). The putatively disrupted boundaries exhibit higher DNA methylation and lower CTCF binding in *IDH* mutant tumors, relative to wildtype (Extended Data Fig. 1). These data suggest that the methylator phenotype disrupts CTCF binding and domain boundaries, thereby affecting gene expression in *IDH* mutant gliomas.

Author Manuscript Author Manuscript Author Manuscript Author Manuscript

We hypothesized that altered domain topologies might contribute to gliomagenesis by activating oncogenes that are normally insulated by domain boundaries. We therefore scanned the domains adjacent to the disrupted boundaries for genes with higher expression in *IDH* mutant than wild-type gliomas (Figure 2a). Genes in top scoring domains include *PDGFRA* ($p<10^{-21}$), an established glioma oncogene[22], and other candidate regulators of gliomagenesis (Table S1).

The identification of *PDGFRA* as a potential target of epigenetic deregulation in *IDH* mutants was of particular interest, given its prominence as a glioma oncogene and established roles for PDGFA signaling in normal brain. Although *PDGFRA* is a frequent target of genomic amplification and gain-of-function mutations in glioblastoma (15%), such alterations are rare in *IDH* mutant tumors[23,24]. Nonetheless, *IDH* mutant gliomas strongly express *PDGFRA* (Fig. 2b), and share the proneural transcriptional program characteristic of *PDGFRA*-amplified tumors[23,24]. Closer examination of expression patterns in *IDH* mutant gliomas reveals a striking correlation between *PDGFRA* and *FIP1L1*, despite an intervening boundary (Fig. 2c). *FIP1L1* encodes an RNA processing protein that is constitutively expressed in neural tissues, and particularly active in oligodendrocyte precursors, a putative glioma cell-of-origin[22] (Extended Data Fig. 2a). Moreover, combined expression of *PDGFRA* and *FIP1L1* is associated with poorer outcome in *IDH* mutant lower-grade gliomas (Extended Data Fig. 2b). This suggests that an aberrant interaction with this constitutive locus may drive *PDGFRA* expression in *IDH* mutant tumors.

We therefore investigated the topology of the region using kilobase-resolution HiC data[15]. In all six cell types examined, *PDGFRA* and *FIP1L1* reside in distinct domains, separated by one CTCF-anchored constitutive boundary (Fig. 3a, Extended Data Fig. 3). Our ChIP-seq data confirm that this boundary contains a strong CTCF binding site over a canonical CTCF motif with a CpG dinucleotide in a position previously linked to methylation-sensitivity[25] (Fig. 3b). Quantitative ChIP-PCR reveals that CTCF occupancy at this site is reduced between 30% and 50% in *IDH* mutant tumors and gliomasphere models, relative to wildtype (Fig. 3c,d). Moreover, the CpG in this motif becomes highly methylated in *IDH* mutants (Fig. 3e,f). This suggests that reduced CTCF binding may compromise the boundary flanking *PDGFRA* in *IDH* mutant, hyper-methylated tumors.

To identify regulatory elements that might underlie *PDGFRA* induction, we mapped the enhancer-associated histone modification, H3 lysine 27 acetylation (H3K27ac), in glioma specimens and models. We identified a large enhancer ~50 kb upstream of *FIP1L1* with strong acetylation in wildtype and mutant tumors (Fig. 3a; Extended Data Fig. 4). In support of an enhancer identity, the element is enriched for H3 lysine 4 mono-methylation (H3K4me1), but lacks H3K4me3, and contains conserved motifs bound by the glioma master transcription factors, OLIG2 and SOX2. Although this enhancer is normally insulated from *PDGFRA*, we reasoned that disruption of the intervening boundary might allow it to interact with the oncogene in *IDH* mutant gliomas. To test this, we used chromosome conformation capture (3C) to query the relative frequencies with which the *PDGFRA* promoter interacts with the *FIP1L1* enhancer, with an intragenic *PDGFRA* enhancer, or with nearby control sites (Fig. 3g). We fixed *IDH* mutant and wildtype glioma specimens and gliomaspheres, digested their chromatin with HinDIII, and performed proximity ligation to

Author Manuscript Author Manuscript Author Manuscript Author Manuscript

re-ligate physically interacting DNA sequences. We used qPCR to measure ligation frequencies between elements, normalizing against control ligations performed with bacterial artificial chromosome DNA.

In wildtype gliomas, 3C revealed a strong interaction between the *PDGFRA* promoter and its intragenic enhancer, which are ~50 kb apart (Fig. 3j,k). In contrast, the *PDGFRA* promoter does not interact with the *FIP1L1* enhancer in wildtype tumors, consistent with retention of the intervening boundary (Fig 3h,i). However, the interaction patterns were markedly different in *IDH* mutant tumors. Here, 3C revealed a strong interaction between the *PDGFRA* promoter and the *FIP1L1* enhancer, despite a separation of ~900 kb (Fig. 3i). For comparison, this interaction is ~5-fold stronger than that between *PDGFRA* promoter and its intragenic enhancer. To confirm this interaction, we designed and normalized reciprocal probe and primers to compare the relative strength with which the *FIP1L1* enhancer interacts with nearby promoters and *PDGFRA* (Extended Data Fig. 5). Remarkably, we found that the *FIP1L1* enhancer-*PDGFRA* promoter interaction is stronger than the *FIP1L1* enhancer-*FIP1L1* promoter interaction in *IDH* mutant tumors. This suggests that disruption of a boundary element by *IDH* mutation and hyper-methylation allows a potent constitutive enhancer to aberrantly interact with, and up-regulate *PDGFRA*.

To test this model functionally, we considered whether perturbing the boundary alters *PDGFRA* expression in patient-derived gliomaspheres (Fig. 4a). First, we focused on the *IDH1* mutant oligoastrocytoma model, BT142. In this mutant line, the CpG dinucleotide in the CTCF motif exhibits higher methylation than wildtype models (~13% vs ~2% per bisulfite sequencing), and CTCF binding is ~3-fold lower. Consistently, 3C reveals a strong interaction between *FIP1L1* enhancer and *PDGFRA* promoter that is specific to the mutant line (Fig. 3i), and *PDGFRA* is highly expressed.

We reasoned that demethylating agent should reduce methylation at this CpG dinucleotide, allowing CTCF to bind and restore *PDGFRA* insulation. We therefore treated BT142 gliomaspheres with the DNA methyltransferase inhibitor 5-azacytidine (5-aza). 5-aza treatment reduced methylation of the CTCF motif by ~2.5-fold, increased CTCF occupancy by ~1.7-fold and down-regulated *PDGFRA* expression by ~5-fold (Fig. 4b–d). These results directly implicate DNA hyper-methylation in compromising CTCF binding, boundary function and oncogene insulation in *IDH* mutant tumors.

Finally, we investigated whether genetic disruption of the CTCF motif could induce *PDGFRA* expression in wildtype gliomaspheres with an intact boundary (Fig. 4a). Here we focused on GSC6, a patient-derived glioblastoma model that harbors an EGFR amplification, but is wildtype for *IDH* and *PDGFRA*. We sought to disrupt the CTCF site in the boundary by CRISPR-based genome engineering (Fig. 4e)[26,27]. We designed a short guide RNA (sgRNA) with a protospacer adjacent motif (PAM) within the CTCF motif. We used a single-vector lentiviral delivery system to infect GSC6 with a Cas9 expression construct containing this insulator sgRNA or a control sgRNA (targeting GFP). Surveyor assay confirmed target locus disruption in the insulator CRISPR condition (Fig. 4f). Direct sequencing of the target locus revealed that ~25% of alleles in the insulator CRISPR

Author Manuscript Author Manuscript Author Manuscript Author Manuscript

gliomaspheres contain a deletion within the CTCF motif expected to disrupt binding, compared to <0.1% in the GFP control (Fig. 4g,h).

We quantified *PDGFRA* expression in the genetically modified gliomaspheres. RT-PCR revealed a ~1.6-fold increase in *PDGFRA* mRNA in the insulator CRISPR cells, relative to control (Fig. 4i). Similarly, flow cytometry revealed a ~1.8-fold increase in the fraction of cells with PDGFRa surface expression (Fig. 4j). We conservatively estimate that CTCF motif disruption causes a ~3-fold increase in *PDGFRA* expression, given that DNA level analysis indicates that <50% of insulator CRISPR cells were successfully edited.

Finally, we considered whether CRISPR-mediated boundary disruption and *PDGFRA* induction affects gliomasphere fitness. In support, the insulator CRISPR gliomaspheres have a ~2-fold growth advantage over the control GFP CRISPR gliomaspheres (Fig. 4k). This growth advantage is dependent on PDGFRa signaling, as it is abrogated by treatment with PDGFR inhibitors, dasatinib or crenolanib (Fig. 4k, Extended Data Fig. 6). Notably, *PDGFRA* expression in insulator CRISPR gliomaspheres increased further after extended culture (to 2-fold over control), potentially due to selection of effectively edited clones. The observation that genetic disruption of this CTCF boundary element induces *PDGFRA* expression and enhances proliferation provides strong support for our model that epigenetic disruption of this element offers similar growth advantage to *IDH* mutant gliomas.

In conclusion, we present a novel epigenetic mechanism by which gain-of-function *IDH* mutations induce *PDGFRA* expression and thereby promote fitness in a subset of gliomas. We specifically find that, in addition to familiar effects on CpG islands, *IDH* mutations cause hyper-methylation of CTCF binding sites genome-wide. This is associated with reduced CTCF binding and a global deregulation of boundary elements that partition topological domains. Disruption of a specific boundary bordering *PDGFRA* allows a potent enhancer to aberrantly contact and activate this canonical glioma oncogene.

Although disruption of this single boundary confers a growth advantage, it is unlikely to be the only mediator of *IDH* mutations in gliomas. The widespread disruption of CTCF binding and boundary element function could provide many opportunities for oncogene deregulation, and subsequent selection of proliferative progeny that inherit the altered epigenetic state. Insulator dysfunction may also be accompanied by promoter silencing events[28,29], and by alterations to other pathways affected by 2-HG[7,30]. Conversely, disruption of chromosomal topology and oncogene insulation may be more generally relevant to methylator phenotypes observed in colorectal and renal cell carcinomas, leukemia and other malignancies[28].

Methods and Materials

Primary glioma specimens and gliomasphere models

Clinical samples GBM1w, GBM2w, GBM3w, GBM4w, GBM5w, GBM6w, GBM7w, AA15m, AA16m, AA17m, OD18m, and AA19m were obtained as frozen specimens from the Massachusetts General Hospital Pathology Tissue Bank or received directly after surgical resection and flash frozen (Extended Data Table 1). All samples were acquired with Institutional Review Board approval, and were deidentified prior to receipt. GBM1w was

Author Manuscript Author Manuscript Author Manuscript Author Manuscript

obtained at autopsy; the remaining samples were surgical resections. *IDH1* status was determined for all clinical samples by SNaPshot multiplex PCR[31]. *PDGFRA* status was confirmed by FISH analysis. Tissue (200–500 μg) was mechanically minced with a sterile razor blade prior to further processing.

Gliomaspheres were maintained in culture as described[32,33]. Briefly, neurosphere cultures contain Neurobasal media supplemented with 20 ng/mL recombinant EGF (R and D Systems), 20ng/mL FGF2 (R and D Systems), 1X B27 supplement (Invitrogen), 0.5X N2 supplement (Invitrogen), 3mM L-glutamine, and penicillin/streptomycin. Cultures were confirmed to be mycoplasma-free via PCR methods. GSC4 and GSC6 gliomasphere lines were derived from *IDH1* wildtype tumors resected at Massachusetts General Hospital, and have been previously described and characterized[32–34]. BT142 gliomasphere line (*IDH1* mutant)[35] was obtained from ATCC, and cultured as described above except 25% conditioned media was carried over each passage. BT142 G-CIMP status was confirmed by evaluating LINE methylation with the "Global DNA Methylation Assay – LINE-1″ kit (Active Motif), as described[36], and by methylation-sensitive restriction digests. GSC119 was derived from an *IDH1* mutant tumor (confirmed by SNaPsShot) resected at Massachusetts General Hospital. We confirmed *IDH1* mutant status of GSC119 by RNA-seq (82 out of 148 reads overlapping the relevant position in the transcript correspond the mutant allele). The gliomasphere models were derived from tumors of the following type: GSC4, GSC6 – primary glioblastoma, BT142 – grade III oligoastrocytoma, GSC119 – secondary glioblastoma, G-CIMP. Clinical specimens and models used in this study are detailed in Extended Data Table 1.

Chromatin Immunoprecipitation

Chromatin Immunoprecipitation (ChIP) and sequencing (ChIP-Seq) was performed as described previously[32]. Briefly, cultured cells or minced tissue was fixed in 1% formaldehyde and snap frozen in liquid nitrogen and stored at −80°C for at least overnight. Sonication of tumor specimens and gliomaspheres was calibrated such that DNA was sheared to between 400bp and 2000bp. CTCF was immunoprecipitated with a monoclonal rabbit CTCF antibody, clone D31H2 (Cell Signaling 3418). H3K27ac was immunoprecipitated with an antibody from Active Motif (cat 39133). ChIP DNA was used to generate sequencing libraries by end repair (End-It DNA repair kit, Epicentre), 3′ A base overhang addition via Klenow fragment (NEB), and ligation of barcoded sequencing adapters. Barcoded fragments were amplified via PCR. Libraries were sequenced as 38 base paired-end reads on an Illumina NextSeq500 instrument or as 50 base single-end reads on a MiSeq instrument. Sequencing libraries are detailed in Extended Data Table 2. H3K27ac maps for GSC6 were previously published deposited to GEO as GSM1306340. Genomic data has been deposited into GEO as GSE70991.

For sequence analysis, identical reads were collapsed to a single paired-end read in order to avoid PCR duplicates. In order to avoid possible saturation, reads were downsampled to 5% reads collapsed as PCR duplicates, or 5 million fragments. Reads were aligned to hg19 using BWA, and peaks were called using HOMER. ChIP-seq tracks were visualized using Integrative Genomics Viewer (IGV, http://www.broadinstitute.org/igv/). To detect peaks lost

Author Manuscript Author Manuscript Author Manuscript Author Manuscript

in *IDH* mutants, we called signal over all peaks in a 100bp window centered on the peaks. To control for copy number changes, we first called copy number profiles from input sequencing data using CNVnator[37]. We then removed all regions where at least one sample had a strong deletion (<0.25), and normalized by copy number. To account for batch effects and difference in ChIP efficiency, we quantile normalized each dataset. Peaks were scored as lost or gained if the difference in signal between a given tumor and the average of the five wildtype tumors was at least 2-fold lower or higher, with a signal of at least 1 in all wildtype or all *IDH* mutant tumors. Fisher exact test confirmed that the overlap between peaks lost in the *IDH* mutant tumors is highly significant ($p<10^{-100}$).

GC content over CTCF peaks lost (or retained) in the *IDH1* mutant glioma specimens was averaged over 200bp windows centered on each peak lost in *IDH* mutant tumors. Methylation levels were quantified over these same regions for 3 *IDH* mutant and 3 *IDH* wildtype tumors, using TCGA data generated by whole genome bisulfite sequencing[10]. Briefly, methylation levels (%) based on proportion of reads with protected CpG were averaged over all CpG dinucleotides in these regions, treating each tumor separately.

Occupancy of the CTCF site in the boundary element adjacent to the PDGFRA locus was quantified by ChIP qPCR, using the following primers: PDGFRActcfF: 5′-GTC ACA GTA GAA CCA CAG AT -3′, PDGFRActcfR: 5′-TAA GTA TAC TGG TCC TCC TC -3′. Equal masses of ChIP or input (WCE) DNA were used as input for PCR, and CTCF occupancy was quantified as a ratio between ChIP and WCE, determined by 2^-deltaCT. CTCF peak intensity was further normalized as ratio to two invariant peaks, at *PSMB1* and *SPG11*, using the following primers: PSMB1ctcfF – 5′-CCT TCC TAG TCA CTC AGT AA -3′, PSMB1ctcfR – 5′-CAG TGT TGA CTC ATC CAG -3′, SPG11ctcfF – 5′-CAG TAC CAG CCT CTC TAG -3′, SPG11ctcfR – 5′-CTA AGC TAG GCC TTC AAG -3′.

Cross-Boundary and Intra-Domain Gene Pair Correlation Analysis

RNA-seq data for 357 normal brain samples was downloaded from GTEx[20]. RNA-seq data and copy number profiles for lower grade gliomas were downloaded from TCGA[23,24]. Contact domains of IMR90, GM12878, K562 and NHEK cells were obtained from published HiC data[15]. Genes were assigned to the inner most domain their transcription start site fell within. Gene pairs were considered to be in the same domain if they were assigned to the same domain in both GM12878 and IMR90. Gene pairs were considered to span a boundary if they were assigned to different domains in both GM12878 and IMR90, and separated by a CTCF binding site in *IDH* wild type tumors. Gene pairs that did not fit either criterion were excluded from this analysis. The plot of correlation vs distance for brain GTEx samples is based on Pearson correlations for all relevant pairs, smoothed by locally weighted scatterplot smoothing with weighted linear least squares (LOESS). To assess the bias in correlation differences, we computed the difference of Pearson correlations between wild-type and *IDH* mutant gliomas for all gene pairs separated by <180 kb. In Figure 1e, this difference in correlations is plotted against the significance of this difference (estimated by Fisher z-transformation). For each gene pair, we omitted samples with a deletion or amplification of one of the genes at or above threshold of the minimal arm level deletion or amplification (to avoid copy number bias). To ensure robustness, we also repeated the

Author Manuscript Author Manuscript Author Manuscript Author Manuscript

analysis using boundaries defined from HiC data for K562 and NHEK. This yielded similar results: 84% pairs gaining correlation cross boundary vs. 71% expected ($p<8*10^{-3}$), 54% pairs losing correlation are within the same domain vs. 29% expected ($p<3*10^{-8}$). Repeating the analysis with only the 14,055 genes that have expressed over 1 TPM in at least half the samples also yielded similar results (Extended Data Fig. 7): 92% pairs gaining correlation cross boundary vs. 69% expected ($p<2*10^{-3}$), 73% pairs losing correlation are within the same domain vs. 31% expected ($p<8*10^{-4}$).

Genomic Scan for Deregulated Boundaries

To detect boundaries deregulated in *IDH* mutant gliomas, we scanned for gene pairs, separated by <1MB, with a significant difference in correlation between wild-type and *IDH* mutant tumors (Fisher z-transformation, FDR<1%). We omitted amplified or deleted samples as described above. To ensure robustness to noise from lowly expressed genes, we first filtered out 6,476 genes expressed < 1 TPM in more than half of the samples (keeping 14,055 genes). We considered all domains and boundaries scored in IMR90 HiC data[13]. Gene pairs crossing a CTCF peak and an IMR90 boundary (i.e. can be assigned to different domains) that were significantly more correlated in *IDH* mutant tumors were considered to support the loss of that boundary. Gene pairs not crossing a boundary (i.e. can be assigned to the same domain) that were significantly less correlated in *IDH* mutant tumors were considered to support the loss of a flanking boundary. We collated a set of deregulated boundaries, supported by at least one cross-boundary pair gaining correlation and at least one intra-domain pair losing correlation. Each was assigned a p-value equal to the product of both supporting pairs (best p-value was chosen if there were more supporting pairs). If both boundaries of a domain were deregulated, or if the same pair of gene pairs (one losing and one gaining correlations) were supporting more than one boundary due to overlapping domains the entries were merged (Supplemental Table 1). This definition allows every gene pair to be considered as potential support for a boundary loss. To quantify CTCF occupancy over these deregulated boundaries, we averaged the signal over all CTCF peaks located within a 1 kb window around the boundary, using copy number and quantile normalized CTCF signals. To quantify DNA methylation over the deregulated boundaries, we averaged DNA methylation signals from TCGA data in 200bp windows as above. Figure 2a depicts significance of disrupted domains and the fold-change of genes in them that are upregulated in *IDH* mutant tumors (compared to median expression in wild-type). In addition to *PDGFRA*, top ranking genes include *CHD4* ($p<10^{-32}$), a driver of glioblastoma tumor initiation[38], *L1CAM* ($p<10^{-8}$), a regulator of the glioma stem cells and tumor growth[39], and other candidate regulators (Supplemental Table 1).

To ensure robustness to cell type-specific boundaries, we repeated the analysis with GM12878, K562 and NHEK defined boundaries. This yielded very similar results, and again highlighted PDGFRA as an over-expressed gene adjacent to a disrupted boundary.

TCGA Correlation and Outcome Analysis

For the correlation of *FIP1L1* and *PDGFRA* expression, RNAseq data from the TCGA Lower Grade Glioma (LGG) and Glioblastoma (GBM) datasets[2,24] were downloaded and segregated by IDH1 mutation status and subtype. Patients from the proneural subtype were

Author Manuscript Author Manuscript Author Manuscript Author Manuscript

divided by *IDH* mutation status, while patients from the mesenchymal, classical, or neural subtypes (which had no IDH mutations) were classified as "Other." For correlation analysis, patients with copy number variation in either gene were excluded from the analysis to control for effects of co-amplification. For outcome analysis, LGG RNAseq data and corresponding patient survival data was obtained from TCGA. Patients with sum *PDGFRA* and *FIP1L1* expression of at least one half of one standard deviation above the mean were classified as "high *PDGFRA* and *FIP1L1* expression" (n=17) while all other patients were classified as "low *PDGFRA* and *FIP1L1* expression" (n=201). Data were plotted as Kaplan-Meier curves and statistically analyzed via logrank test.

HiC Data Analysis and Visualization

HiC data[15] was downloaded from GEO. 5 kb resolution intra-chromosomal contact scores for Chromosome 4 for the cell lines IMR90, NHEK, KBM7, K562, HUVEC, HMEC, and GM12878 were filtered to the region between 53,700kb and 55,400kb. The average interaction score at each coordinate pair for all cell lines was calculated and used to determine putative insulator elements as local maxima at the interaction point of two domain boundaries. In order to determine the interactions of the *PDGFRA* promoter, the interaction scores of all points in the region with the PDGFRA promoter (chr4:55,090,000) were plotted as a one-dimensional trace. In order to view the topological domain structure of the region, HiC interaction scores were visualized using Juicebox (http://www.aidenlab.org/juicebox/)[15]. Data shown is from the IMR90 cell line at 5kb resolution, normalized to coverage.

DNA Methylation Quantification

DNA methylation was analyzed in two ways. For gliomaspheres, genomic DNA was isolated via QiaAmp DNA minikit (Qiagen) and subjected to Bisulfite Conversion (EZ DNA Methylation Gold Kit – Zymo Research). Bisulfite converted DNA specific to the CTCF binding site (defined by JASPAR[40]) in the boundary adjacent to *PDGFRA* was amplified using the following primers F: 5′-GAA TTA TAG ATA ATG TAG TTA GAT GG -3′, R: 5′-AAA TAT ACT AAT CCT CCT CTC CCA AA -3′. Amplified DNA was used to prepare a sequencing library, which was sequenced as 38 base paired-end reads on a NextSeq500. For tumors, limiting DNA yields required an alternate strategy for methylation analysis. Tumor genomic DNA was isolated from minced frozen sections of tumors by QiaAmp DNA minikit (Qiagen). Genomic DNA was digested using the methylation-sensitive restriction enzyme Hin6I (Thermo) recognizing the restriction site GCGC, or subjected to mock digestion. Protected DNA was quantified by PCR using the following primer set: PDGFRAinsF: 5′-CGT GAG CTG AAT TGT GCC TG -3′, PDGFRAinsR: 5′-TGG GAG GAC AGT TTA GGG CT -3′, normalizing to mock digestion.

Chromatin Conformation Capture (3C)

3C analysis was performed using procedures as described previously[41,42]. Briefly, ~10 million cell equivalents from minced tumor specimens or gliomasphere cultures were fixed in 1% formaldehyde. Fixed samples were lysed in lysis buffer containing 0.2% PMSF using a Dounce Pestle. Following lysis, samples were digested with HinDIII (NEB) overnight on a thermomixer at 37°C rotating at 950 RPM. Diluted samples were ligated using T4 DNA

Author Manuscript Author Manuscript Author Manuscript Author Manuscript

ligase (NEB) at 16°C overnight, followed by RNase and Proteinase K treatment. DNA was extracted via phenol/chloroform/isoamyl alcohol (Invitrogen). DNA was analyzed via TaqMan PCR using ABI master mix. Primers and probe were synthesized by IDT with the following sequences: Common PDGFRA Promoter: 5′-GGT CGT GCC TTT GTT TT -3′, FIP1L1 Control: 5′-CAG GGA AGA GAG GAA GTT T -3′, FIP1L1 Enhancer: 5′-TTA AGT AAG CAG GTA AAC TAC AT -3′, Intragenic Enhancer: 5′-AGC CTT TGC CTC CTT TT -3′, Intragenic Control: 5′-CCA CAG GGA GAA GGA AAT -3′, Intact Promoter: 5′-CAA GGA ATT CGT AGG GTT C -3′, Probe: 5′-/56-FAM/TTG TAT GCG/ZEN/AGA TAG AAG CCA GGG CAA/3IABkFQ/-3′. For the reciprocal FIP1L1 enhancer interaction interrogation, the following primer sequences were used: Common Enhancer Primer – as FIP1L1 Enhancer Primer above (5′-TTA AGT AAG CAG GTA AAC TAC AT -3′), PDGFRA Promoter – as Common PDGFRA Promoter above (5′-GGT CGT GCC TTT GTT TT -3′), SCFD2 Promoter - 5′-AAT ACA TGG TCA TGA TGC TC -3′, FIP1L1 Promoter - 5′-AGG CAT TGC TTA AAC ATA AC -3′, FIP1L1 control - 5′-TTA TTT GTA GTA GAG GTT ACT GG -3′, PDGFRA control - 5′-ATG ATA ACA CCA CCA TTC AG -3′, FIP1L1 enhancer Probe - 5′-/56-FAM/TAT CCC AAC/ZEN/CAA ATA CAG GGC TTG G/3IABkFQ/-3′. In order to normalize primer signals, Bacterial Artificial Chromosome (BAC) clones CTD-2022B5 and RP11-626H4 were obtained from Invitrogen. BAC DNA was purified via BACMAX DNA Purification kit (Epicenter) and quantified using two primer sets specific to the Chloramphenicol resistance gene: 1F: 5′-TTC GTC TCA GCC AAT CCC TG -3′, 1R: 5′-TTT GCC CAT GGT GAA AAC GG -3′, 2F: GGT TCA TCA TGC CGT TTG TG -3′, 2R: 5′-CCA CTC ATC GCA GTA CTG TTG -3′. BAC DNA was subjected to a similar 3C protocol, omitting steps related to cell lysis, proteinase or RNase treatment. PCR signal from tumor and gliomasphere 3C was normalized to digestion efficiency and BAC primer signal.

Treatment with demethylating agent

BT142 cells were cultured in either 5μM 5-azacytidine or equivalent DMSO (1:10,000) for 8 days, with drug refreshed every 2 days.

CRISPR/Cas9 Insulator Disruption

The following CRISPR small guide RNAs were cloned into the LentiCRISPR vector obtained from the Zhang lab[43]: GFP: 5′-GAG CTG GAC GGC GAC GTA AA -3′, Insulator: 5′-GCC ACA GAT AAT GCA GCT AGA -3′. GSC6 gliomaspheres were mechanically dissociated and plated in 5 μg/mL EHS Laminin (Sigma) and allowed to adhere overnight and then infected with lentivirus containing either CRISPR vector for 48h. Cells were then selected in 1μg/mL puromycin for four days, with puromycin-containing media refreshed every two days. Genomic DNA was isolated and the region of interest was amplified using the PDGFRAins primer set described above. CRISPR-mediated disruption of this amplified DNA was confirmed via Surveyor Assay (Transgenomic), with amplified uninfected GSC6 genomic DNA being added to each annealing reaction as the unmodified control. In order to quantify the precise CRISPR alterations, genomic DNA from each construct was amplified using a set of primers closer to the putative deletion site as follows: F: 5′-TTT GCA ATG GGA CAC GGA GA -3′, R: 5′-AGA AAT GTG TGG ATG TGA GCG -3′. PCR product

Author Manuscript Author Manuscript Author Manuscript Author Manuscript

from these primers was used to prepare a library that was sequenced as 38 base paired-end reads on the Illumina NextSeq500.

PDGFRA Quantitative PCR

Total RNA was isolated from CRISPR-infected GSC6 gliomaspheres (Insulator or control GFP sgRNA) or BT142 gliomaspheres (5-aza treated or control condition) using the RNeasy minikit (Qiagen) and used to synthesize cDNA with the SuperScriptIII system (Invitrogen). cDNA was analyzed using SYBR mastermix (Applied Biosystems) on a 7500 Fast Real Time System (Applied Biosystems). PDGFRA expression was determined using the following primers: F: 5′-GCT CAG CCC TGT GAG AAG AC -3′, R: 5′-ATT GCG GAA TAA CAT CGG AG -3′, and was normalized to primers for Ribosomal Protein, large, P0 (RPLP0), as follows: F: 5′-TCC CAC TTG CTG AAA AGG TCA -3′, R: 5′-CCG ACT CTT CCT TGG CTT CA -3′. Normalization was also verified by β-actin, F: 5′-AGA AAA TCT GGC ACC ACA CC -3′, R: 5′-AGA GGC GTA CAG GGA TAG CA -3′.

PDGFRA Flow Cytometry

Cells were incubated with PE-conjugated anti-PDGFRA (CD140a) antibody (Biolegend, clone 16A1) for 30 minutes at room temperature at the dilution specified in the manufacturer's protocol. Data was analyzed and visualized with FlowJo software. Single live cells were selected for analysis via side and forward scatter, and viable cells were selected by lack of an unstained channel (APC) autofluorescence.

Cell Growth Assay

For the cell growth assay, 2,500 dissociated viable GSC6 cells expressing CRISPR and either GFP or Insulator targeting sgRNA (see above) were plated in 100μL of media in an opaque-walled tissue culture 96 well plate, in 1μM Dasatinib, 500nM Crenolanib, or equivalent DMSO (1:10,000) as a vehicle control. Cell growth was analyzed at days 3, 5, and 7 for Dasatinib, or days 3, 7, and 10 for Crenolanib, using CellTiter-Glo reagent (Promega) following the manufacturer's protocol. Data was normalized across days using an ATP standard curve.

Author Manuscript Author Manuscript Author Manuscript Author Manuscript

Extended Data

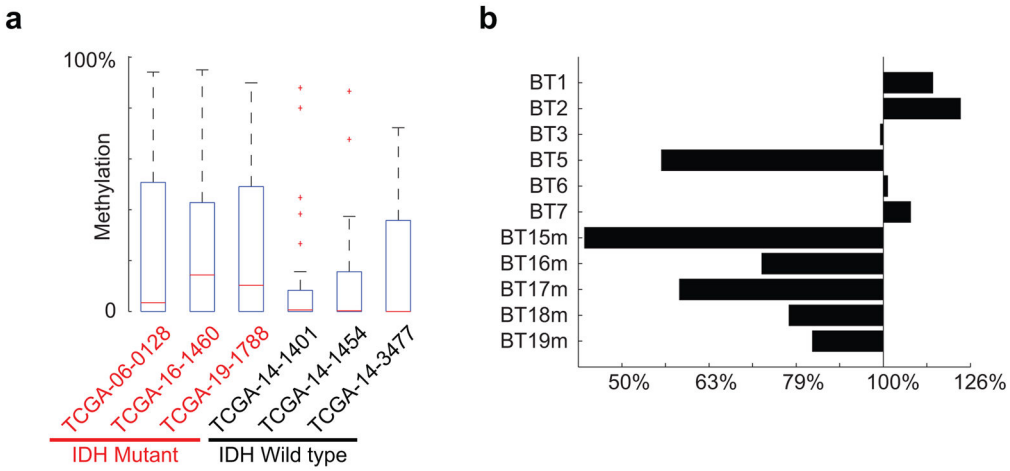

Extended Data Figure 1. DNA methylation and CTCF binding at deregulated boundaries

(**a**) Box plots show DNA methylation levels over CTCF sites (200 bp window centered on the peak) within boundaries predicted by gene pair correlation analysis to be disrupted. All CTCF sites located within a 1 kb window centered on a disrupted boundary were considered. Methylation levels were determined from whole genome bisulfite data for three IDH mutant (red labels) and three IDH wildtype (black labels) tumors. (**b**) Bars show average normalized ChIP-seq signal over all CTCF sites located inside a 1 kb window centered on a disrupted boundary.

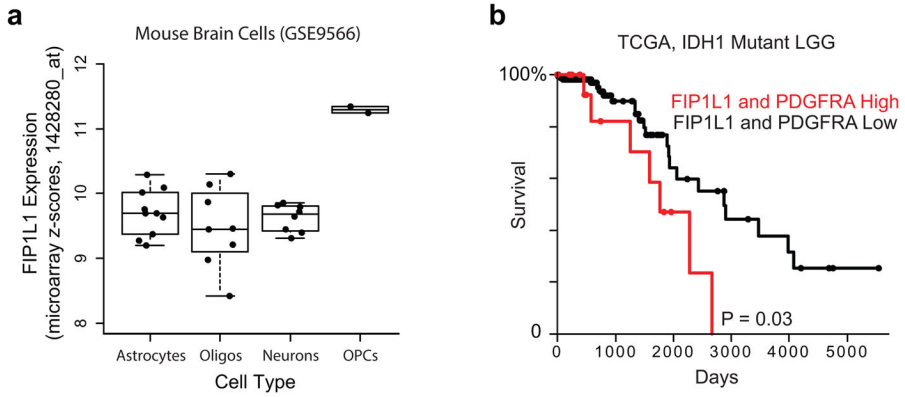

Extended Data Figure 2. Expression of *FIP1L1* in mouse brain cells and survival effects of *PDGFRA* and *FIP1L1*

(**a**) Expression of FIP1L1 in isolated mouse brain cell types[44]. (**b**) Kaplan-Meier Plot based on TCGA data3 indicates that combined FIP1L1 and PDGFRA expression is a negative prognostic factor in IDH1 mutant lower-grade gliomas. Multivariate analysis including the known prognostic factor 1p/19q deletion diminished this effect into non-significance, suggesting that other predictors of survival may also play a role in this model.

Author Manuscript Author Manuscript Author Manuscript Author Manuscript

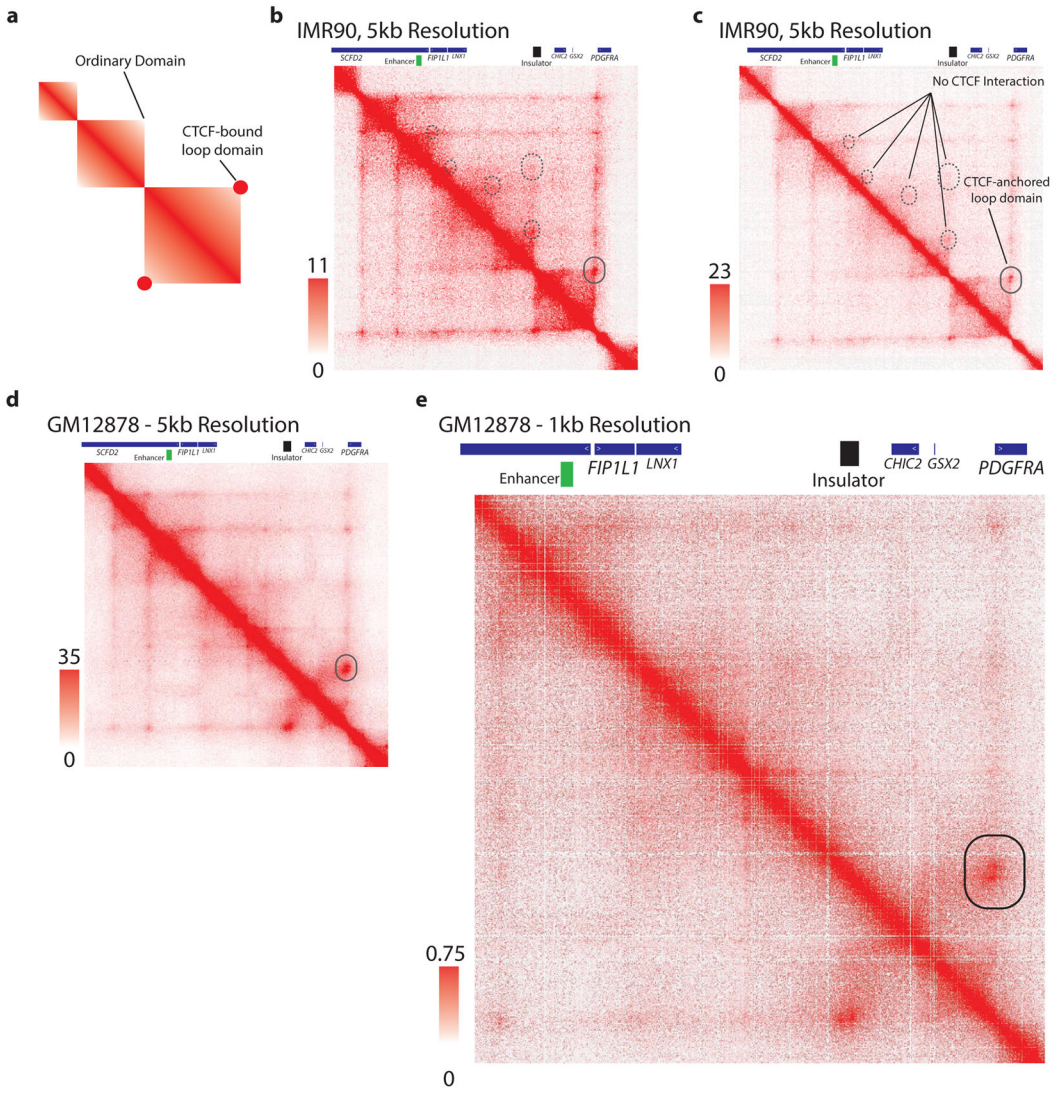

Extended Data Figure 3. CTCF anchored loop in the *PDGFRA* region

(**a**) Schematic depiction of a HiC interaction signature of a CTCF-anchored loop domain, compared to an ordinary domain, as described by Rao et al., *Cell* 2014. CTCF-anchored loop domains are characterized by an increased interaction score at the apex of the domain, representing a CTCF-CTCF dimeric interaction. (**b**) IMR90 HiC contact matrix for the *PDGFRA/FIP1L1* locus, as presented in Figure 3a. Solid circle indicates CTCF dimer interaction point. Dashed circles indicate lack of CTCF dimeric anchor signature. (**c**) IMR90 HiC contact matrix as in (b), but with expanded heatmap scale, more clearly conveys the CTCF-anchored loop that insulates *PDGFRA*. (**d,e**) HiC contact matrix for GM12878 cells for the same region confirms a single CTCF-anchored loop (solid circle) between *PDGFRA* and *FIP1L1*. These data support the significance of this specific boundary in locus topology and *PDGFRA* insulation.

Author Manuscript Author Manuscript Author Manuscript Author Manuscript

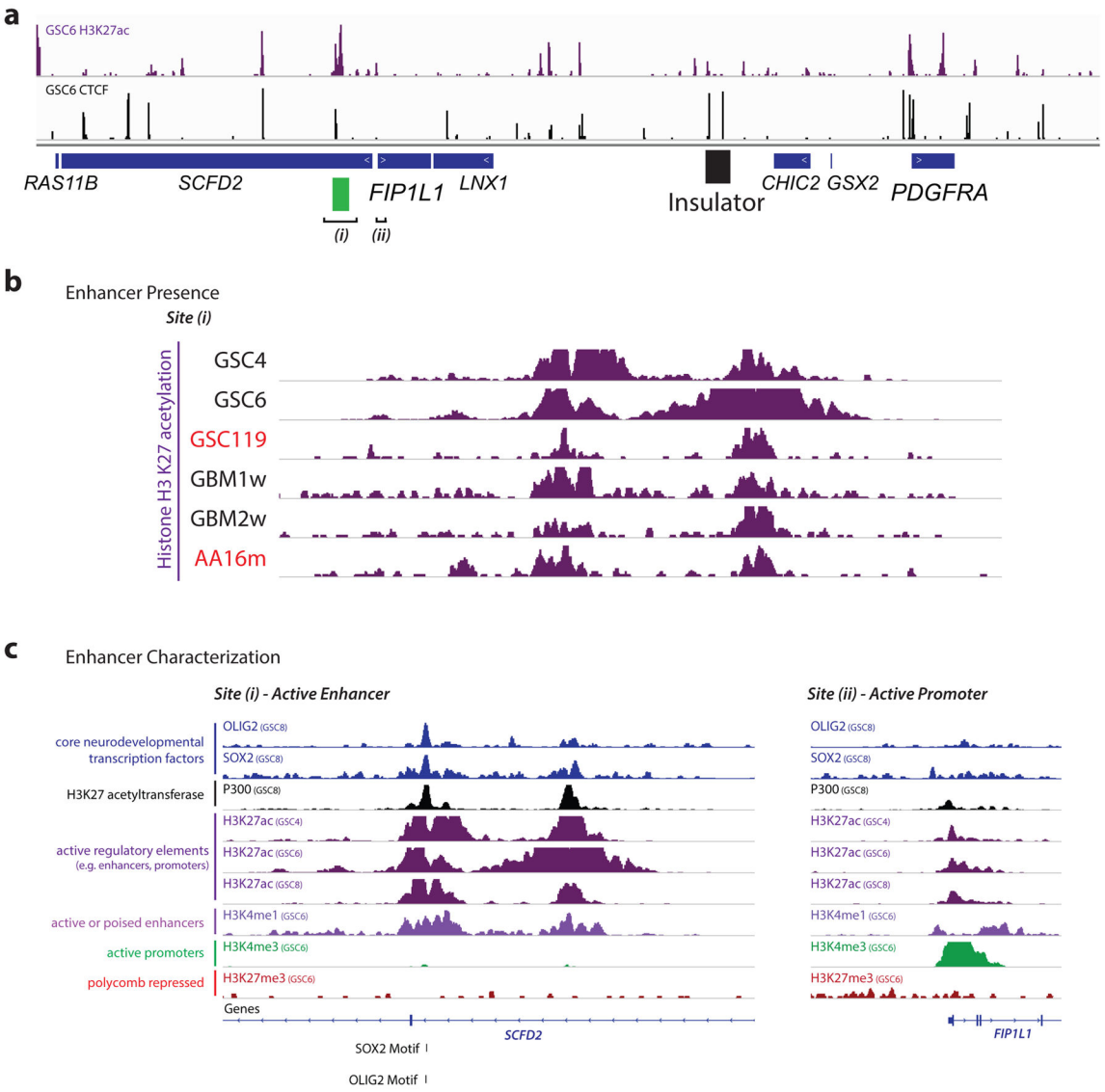

Extended Data Figure 4. Characterization of the *FIP1L1* enhancer

(**a**) H3K27ac ChIP-seq track for GSC6 gliomaspheres reveals strong enrichment over the *FIP1L1* enhancer. CTCF ChIP-seq track reveals location of the boundary element insulator (as in Figure 3a). *FIP1L1* enhancer (*i*) and promoter (*ii*) are indicated. (**b**) H3K27ac ChIP-seq tracks for IDH mutant and wild-type gliomaspheres and glioma specimens reveal enrichment over the FIP1L1 enhancer. (**c**) ChIP-seq tracks for glioma master transcription factors and other histone modifications support the enhancer identity of the element (H3K27ac, H3K4me1, SOX2, OLIG2; lacks H3K4me3, lacks H3K27me3). In contrast, the *FIP1L1* promoter has a distinct ‘promoter-like’ chromatin state.

Author Manuscript Author Manuscript Author Manuscript Author Manuscript

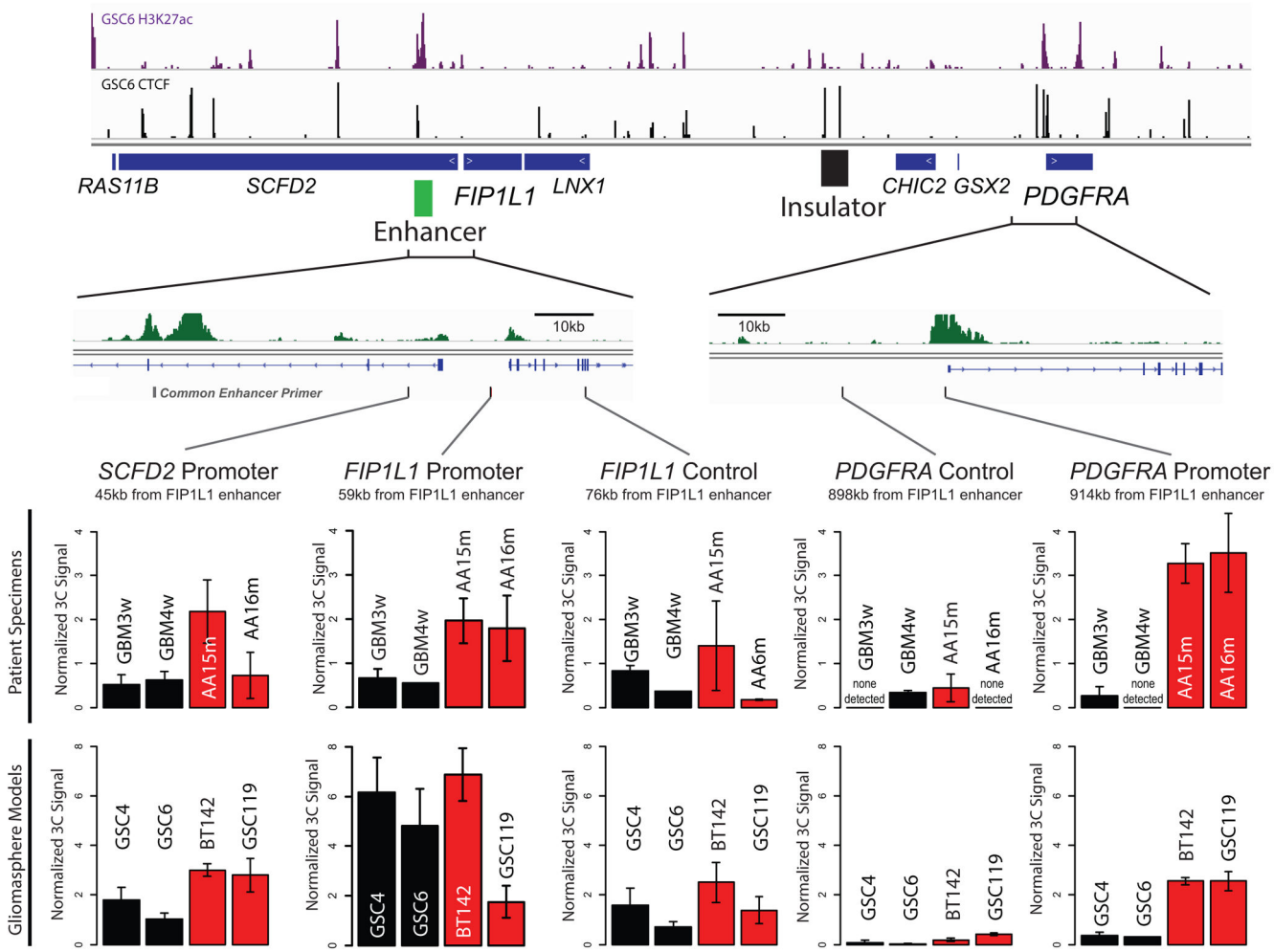

Extended Data Figure 5. Interaction of the FIP1L1 enhancer with nearby promoters and PDGFRA quantified by reciprocal chromatin conformation capture (3C)

(top) The H3K27ac, CTCF and genetic architecture of the *FIP1L1*/*PDGFRA* locus is indicated, highlighting the 3C strategy. (bottom) Plots indicate the interaction signal of the indicated sites (black lines) with the common enhancer primer. The FIP1L1 enhancer interacts with local promoters in wild-type and mutant tumors and models. In *IDH* wild-type gliomas, it shows essentially no interaction with the *PDGFRA* promoter. In *IDH* mutant gliomas, it interacts with the *PDGFRA* promoter with comparable strength to the local interactions, despite the much larger intervening distance (900 kb). Error bars reflect standard deviations.

Author Manuscript Author Manuscript Author Manuscript Author Manuscript

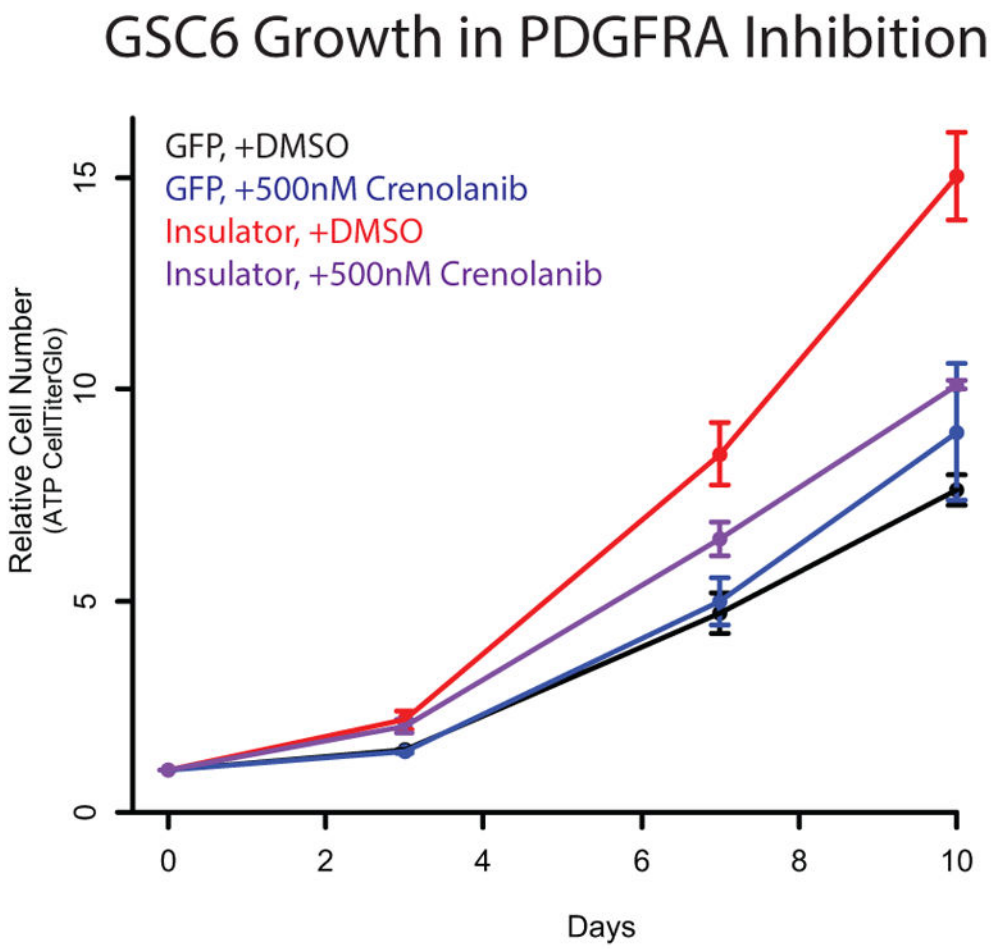

Extended Data Figure 6. Crenolanib reverses the increased growth of *PDGFRA* insulator disrupted cells

Insulator CRISPR-infected gliomaspheres exhibit a roughly 2-fold increase in proliferation rate, compared to control sgRNA infected gliomaspheres. This proliferative advantage is eliminated by treatment with the PDGFRα inhibitor Crenolanib. Crenolanib and Dasatinib both inhibit PDGFRα, but their other targets are non-overlapping. Hence, this sensitivity provides further support that *PDGFRA* induction drives the increased proliferation of the insulator CRISPR gliomaspheres. (Error bars reflect standard deviations).

Author Manuscript Author Manuscript Author Manuscript Author Manuscript

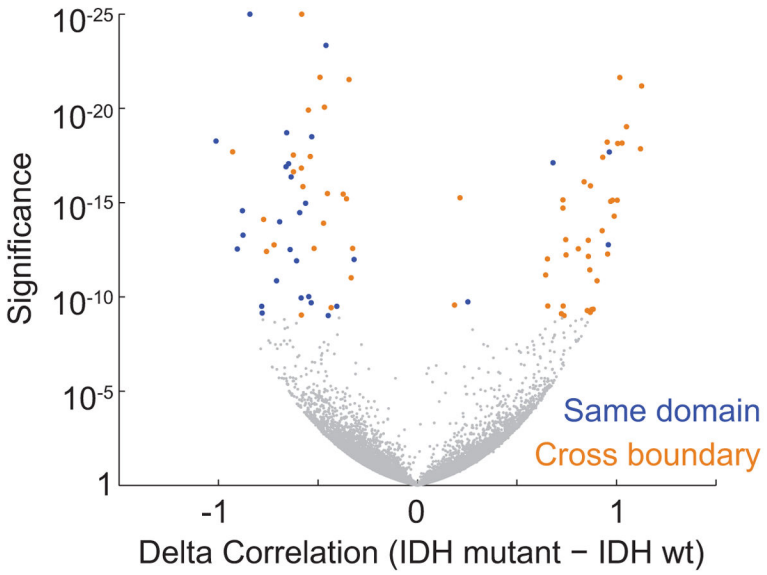

Extended Data Figure 7. Signature of boundary deregulation in *IDH* mutant gliomas is robust

Volcano plot depicts the significance (y-axis) of gene pairs that are either more or less correlated in *IDH* mutant than *IDH* wild-type gliomas. This plot was generated by repeating the analysis in the main text and shown in Figure 1f, except that here the statistics were performed using only the 14,055 genes expressed at >1 TPM in at least half the samples. This indicates that the boundary deregulation signature in *IDH* mutant gliomas is not sensitive to noise from lowly expressed genes.

Extended Data Table 1

Clinical specimens and tumor models.Clinical information for glioma specimens and gliomasphere models is shown.

Glioma	Tissue Type	Tissue Source	Source	IDH1 Status	PDGFRA Status	1p/19q Status	Grade	Disease
GBM1w	Autopsy Specimen	Banked	MGH	Wild Type	Amplified	Not tested	IV	Glioblastoma
GBM2w	Surgical Specimen	Banked	MGH	Wild Type	Wild Type	Not tested	IV	Glioblastoma
GBM3w	Surgical Specimen	Banked	MGH	Wild Type	Wild Type	Not tested	IV	Glioblastoma
GBM4w	Surgical Specimen	Banked	MGH	Wild Type	Wild Type	Not tested	IV	Glioblastoma
GBM5w	Surgical Specimen	Fresh	MGH	Wild Type	Wild Type	Not tested	IV	Glioblastoma
GBM6w	Surgical Specimen	Fresh	MGH	Wild Type	Wild Type	Not tested	IV	Glioblastoma
GBM7w	Surgical Specimen	Fresh	MGH	Wild Type	Wild Type	Not tested	IV	Glioblastoma
AA15m	Surgical Specimen	Banked	MGH	R132H	Wild Type	Intact	III	Anaplastic Astrocyto
AA16m	Surgical Specimen	Banked	MGH	R132H	Wild Type	Intact	III	Anaplastic Astrocyto
AA17m	Surgical Specimen	Fresh	MGH	R132H	Wild Type	Intact	III	Anaplastic Astrocyto
OD18m	Surgical Specimen	Fresh	MGH	R132H	Wild Type	Lost	II	Oligodendroglioma
AA19m	Surgical Specimen	Fresh	MGH	R132H	Wild Type	Intact	III	Anaplastic Astrocyto
GSC4	Gliomasphere	-	MGH	Wild Type	Wild Type	Intact	IV	Glioblastoma
GSC6	Gliomasphere	-	MGH	Wild Type	Wild Type	Intact	IV	Glioblastoma

Author Manuscript Author Manuscript Author Manuscript Author Manuscript

Glioma	Tissue Type	Tissue Source	Source	IDH1 Status	PDGFRA Status	1p/19q Status	Grade	Disease
BT142	Gliomasphere	-	ATCC	R132H	Wild Type	Intact	III	Anaplastic Oligoastrocy
GSC119	Gliomasphere	-	MGH	R132H	Wild Type	Intact	IV	Secondary Glioblasto

Extended Data Table 2

Sequenced Libraries Characteristics.Pertinent statistics are listed for ChIP, genomic DNA, and bisulfite-converted sequencing libraries.

Sample Name	Experiment	Sequencing Depth	Sequencing Format	Sequencing Instrument	Total read number (millions)
GBM1w - CTCF	CTCF ChIP-seq	38 base pairs	Paired end	Illumina NextSeq 500	19.3
GBM2w - CTCF	CTCF ChIP-seq	38 base pairs	Paired end	Illumina NextSeq 500	17.6
GBM3w - CTCF	CTCF ChIP-seq	38 base pairs	Paired end	Illumina NextSeq 500	20.2
GBM5w - CTCF	CTCF ChIP-seq	38 base pairs	Paired end	Illumina NextSeq 500	30
GBM6w - CTCF	CTCF ChIP-seq	38 base pairs	Paired end	Illumina NextSeq 500	35.1
GBM7w - CTCF	CTCF ChIP-seq	38 base pairs	Paired end	Illumina NextSeq 500	36
AA15m - CTCF	CTCF ChIP-seq	38 base pairs	Paired end	Illumina NextSeq 500	8.7
AA16m - CTCF	CTCF ChIP-seq	38 base pairs	Paired end	Illumina NextSeq 500	23.7
AA17m - CTCF	CTCF ChIP-seq	38 base pairs	Paired end	Illumina NextSeq 500	16.3
OD18m - CTCF	CTCF ChIP-seq	38 base pairs	Paired end	Illumina NextSeq 500	9.2
AA19m - CTCF	CTCF ChIP-seq	38 base pairs	Paired end	Illumina NextSeq 500	33
GSC4 - CTCF	CTCF ChIP-seq	38 base pairs	Paired end	Illumina NextSeq 500	19.9
GSC6 - CTCF	CTCF ChIP-seq	38 base pairs	Paired end	Illumina NextSeq 500 Illumina	21.9
BT142 - CTCF	CTCF ChIP-seq	38 base pairs	Paired end	Illumina NextSeq 500	16
GSC119 - CTCF	CTCF ChIP-seq	50 base pairs	Single end	Illumina Miseq	6.39
GBM1w - H3K27ac	H3K27ac ChIP-seq	38 base pairs	Paired end	Illumina NextSeq 500	12.7
GBM2w - H3K27ac	H3K27ac ChIP-seq	38 base pairs	Paired end	Illumina NextSeq 500	10.8
AA15m - H3K27ac	H3K27ac ChIP-seq	38 base pairs	Paired end	Illumina NextSeq 500	11.8
GSC4 - H3K27ac	H3K27ac ChIP-seq	38 base pairs	Paired end	Illumina NextSeq 500	9.7
GSC6 - H3K27ac	H3K27ac ChIP-seq	36 base pairs	Single end	Illumina Hiseq 2500	10.5
GSC119 - H3K27ac	H3K27ac ChIP-seq	38 base pairs	Paired end	Illumina NextSeq 500	9
GSC6 CRISPR - GFP sgRNA	Locus Sequencing	50 base pairs	Single end	Illumina Miseq	0.539
GSC6 CRISPR - insulator sgRNA	Locus Sequencing	50 base pairs	Single end	Illumina Miseq	0.639
GSC4 bisulfite	Bisulfite Sequncing	38 base pairs	Paired end	Illumina NextSeq 500	0.149
GSC6 bisulfite	Bisulfite Sequncing	38 base pairs	Paired end	Illumina NextSeq 500	0.149
BT142 bisulfite	Bisulfite Sequncing	38 base pairs	Paired end	Illumina NextSeq 500	0.149
GSC119 bisulfite	Bisulfite Sequncing	38 base pairs	Paired end	Illumina NextSeq 500	0.156

Author Manuscript Author Manuscript Author Manuscript Author Manuscript

Supplementary Material

Refer to Web version on PubMed Central for supplementary material.

Acknowledgments

We thank James Kim, the MGH Neuro Oncology Tissue Repository, and the MGH Pathology Flow Cytometry Core for assistance with clinical samples and analysis. W.A.F. is supported by a basic research fellowship from the American Brain Tumor Association. B.B.L. is supported by a Jane Coffin Childs fellowship. B.E.B. is an American Cancer Society Research Professor. This research was supported by funds from Howard Hughes Medical Institute, the National Brain Tumor Society and the National Human Genome Research Institute.

References

1. Parsons DW, et al. An integrated genomic analysis of human glioblastoma multiforme. Science. 2008; 321:1807–1812. DOI: 10.1126/science.1164382 [PubMed: 18772396]
2. Cancer Genome Atlas Research N. Comprehensive, Integrative Genomic Analysis of Diffuse Lower-Grade Gliomas. The New England journal of medicine. 2015; 372:2481–2498. DOI: 10.1056/NEJMoa1402121 [PubMed: 26061751]
3. Dang L, et al. Cancer-associated IDH1 mutations produce 2-hydroxyglutarate. Nature. 2009; 462:739–744. DOI: 10.1038/nature08617 [PubMed: 19935646]
4. Figueroa ME, et al. Leukemic IDH1 and IDH2 mutations result in a hypermethylation phenotype, disrupt TET2 function, and impair hematopoietic differentiation. Cancer cell. 2010; 18:553–567. DOI: 10.1016/j.ccr.2010.11.015 [PubMed: 21130701]
5. Xu W, et al. Oncometabolite 2-hydroxyglutarate is a competitive inhibitor of alpha-ketoglutarate-dependent dioxygenases. Cancer cell. 2011; 19:17–30. DOI: 10.1016/j.ccr.2010.12.014 [PubMed: 21251613]
6. Lu C, et al. IDH mutation impairs histone demethylation and results in a block to cell differentiation. Nature. 2012; 483:474–478. DOI: 10.1038/nature10860 [PubMed: 22343901]
7. Cairns RA, Mak TW. Oncogenic isocitrate dehydrogenase mutations: mechanisms, models, and clinical opportunities. Cancer discovery. 2013; 3:730–741. DOI: 10.1158/2159-8290.CD-13-0083 [PubMed: 23796461]
8. Pastor WA, Aravind L, Rao A. TETonic shift: biological roles of TET proteins in DNA demethylation and transcription. Nature reviews. Molecular cell biology. 2013; 14:341–356. DOI: 10.1038/nrm3589 [PubMed: 23698584]
9. Kohli RM, Zhang Y. TET enzymes, TDG and the dynamics of DNA demethylation. Nature. 2013; 502:472–479. DOI: 10.1038/nature12750 [PubMed: 24153300]
10. Noushmehr H, et al. Identification of a CpG island methylator phenotype that defines a distinct subgroup of glioma. Cancer cell. 2010; 17:510–522. DOI: 10.1016/j.ccr.2010.03.017 [PubMed: 20399149]
11. Turcan S, et al. IDH1 mutation is sufficient to establish the glioma hypermethylator phenotype. Nature. 2012; 483:479–483. DOI: 10.1038/nature10866 [PubMed: 22343889]
12. Bickmore WA, van Steensel B. Genome architecture: domain organization of interphase chromosomes. Cell. 2013; 152:1270–1284. DOI: 10.1016/j.cell.2013.02.001 [PubMed: 23498936]
13. Lieberman-Aiden E, et al. Comprehensive mapping of long-range interactions reveals folding principles of the human genome. Science. 2009; 326:289–293. DOI: 10.1126/science.1181369 [PubMed: 19815776]
14. Dixon JR, et al. Topological domains in mammalian genomes identified by analysis of chromatin interactions. Nature. 2012; 485:376–380. DOI: 10.1038/nature11082 [PubMed: 22495300]
15. Rao SS, et al. A 3D map of the human genome at kilobase resolution reveals principles of chromatin looping. Cell. 2014; 159:1665–1680. DOI: 10.1016/j.cell.2014.11.021 [PubMed: 25497547]
16. Nora EP, et al. Spatial partitioning of the regulatory landscape of the X-inactivation centre. Nature. 2012; 485:381–385. DOI: 10.1038/nature11049 [PubMed: 22495304]

Author Manuscript Author Manuscript Author Manuscript Author Manuscript

17. Lupianez DG, et al. Disruptions of topological chromatin domains cause pathogenic rewiring of gene-enhancer interactions. Cell. 2015; 161:1012–1025. DOI: 10.1016/j.cell.2015.04.004 [PubMed: 25959774]
18. Bell AC, Felsenfeld G. Methylation of a CTCF-dependent boundary controls imprinted expression of the Igf2 gene. Nature. 2000; 405:482–485. DOI: 10.1038/35013100 [PubMed: 10839546]
19. Hark AT, et al. CTCF mediates methylation-sensitive enhancer-blocking activity at the H19/Igf2 locus. Nature. 2000; 405:486–489. DOI: 10.1038/35013106 [PubMed: 10839547]
20. Consortium, G. T. Human genomics. The Genotype-Tissue Expression (GTEx) pilot analysis: multitissue gene regulation in humans. Science. 2015; 348:648–660. DOI: 10.1126/science.1262110 [PubMed: 25954001]
21. Zuin J, et al. Cohesin and CTCF differentially affect chromatin architecture and gene expression in human cells. Proceedings of the National Academy of Sciences of the United States of America. 2014; 111:996–1001. DOI: 10.1073/pnas.1317788111 [PubMed: 24335803]
22. Sturm D, et al. Paediatric and adult glioblastoma: multiform (epi)genomic culprits emerge. Nature reviews. Cancer. 2014; 14:92–107. DOI: 10.1038/nrc3655 [PubMed: 24457416]
23. Brennan CW, et al. The somatic genomic landscape of glioblastoma. Cell. 2013; 155:462–477. DOI: 10.1016/j.cell.2013.09.034 [PubMed: 24120142]
24. Verhaak RG, et al. Integrated genomic analysis identifies clinically relevant subtypes of glioblastoma characterized by abnormalities in PDGFRA, IDH1, EGFR, and NF1. Cancer cell. 2010; 17:98–110. DOI: 10.1016/j.ccr.2009.12.020 [PubMed: 20129251]
25. Wang H, et al. Widespread plasticity in CTCF occupancy linked to DNA methylation. Genome research. 2012; 22:1680–1688. DOI: 10.1101/gr.136101.111 [PubMed: 22955980]
26. Hsu PD, Lander ES, Zhang F. Development and applications of CRISPR-Cas9 for genome engineering. Cell. 2014; 157:1262–1278. DOI: 10.1016/j.cell.2014.05.010 [PubMed: 24906146]
27. Sander JD, Joung JK. CRISPR-Cas systems for editing, regulating and targeting genomes. Nature biotechnology. 2014; 32:347–355. DOI: 10.1038/nbt.2842
28. Baylin SB, Jones PA. A decade of exploring the cancer epigenome - biological and translational implications. Nature reviews. Cancer. 2011; 11:726–734. DOI: 10.1038/nrc3130 [PubMed: 21941284]
29. Costello JF, Berger MS, Huang HS, Cavenee WK. Silencing of p16/CDKN2 expression in human gliomas by methylation and chromatin condensation. Cancer research. 1996; 56:2405–2410. [PubMed: 8625319]
30. Koivunen P, et al. Transformation by the (R)-enantiomer of 2-hydroxyglutarate linked to EGLN activation. Nature. 2012; 483:484–488. DOI: 10.1038/nature10898 [PubMed: 22343896]
31. Chi AS, et al. Prospective, high-throughput molecular profiling of human gliomas. Journal of neuro-oncology. 2012; 110:89–98. DOI: 10.1007/s11060-012-0938-9 [PubMed: 22821383]
32. Rheinbay E, et al. An aberrant transcription factor network essential for Wnt signaling and stem cell maintenance in glioblastoma. Cell reports. 2013; 3:1567–1579. DOI: 10.1016/j.celrep.2013.04.021 [PubMed: 23707066]
33. Suva ML, et al. Reconstructing and reprogramming the tumor-propagating potential of glioblastoma stem-like cells. Cell. 2014; 157:580–594. DOI: 10.1016/j.cell.2014.02.030 [PubMed: 24726434]
34. Wakimoto H, et al. Maintenance of primary tumor phenotype and genotype in glioblastoma stem cells. Neuro-oncology. 2012; 14:132–144. DOI: 10.1093/neuonc/nor195 [PubMed: 22067563]
35. Luchman HA, et al. An in vivo patient-derived model of endogenous IDH1-mutant glioma. Neuro-oncology. 2012; 14:184–191. DOI: 10.1093/neuonc/nor207 [PubMed: 22166263]
36. Lai RK, et al. Genome-wide methylation analyses in glioblastoma multiforme. PloS one. 2014; 9:e89376. [PubMed: 24586730]
37. Abyzov A, Urban AE, Snyder M, Gerstein M. CNVnator: an approach to discover, genotype, and characterize typical and atypical CNVs from family and population genome sequencing. Genome research. 2011; 21:974–984. DOI: 10.1101/gr.114876.110 [PubMed: 21324876]
38. Chudnovsky Y, et al. ZFHX4 interacts with the NuRD core member CHD4 and regulates the glioblastoma tumor-initiating cell state. Cell reports. 2014; 6:313–324. DOI: 10.1016/j.celrep.2013.12.032 [PubMed: 24440720]

Author Manuscript Author Manuscript Author Manuscript Author Manuscript

39. Bao S, et al. Targeting cancer stem cells through L1CAM suppresses glioma growth. Cancer research. 2008; 68:6043–6048. DOI: 10.1158/0008-5472.CAN-08-1079 [PubMed: 18676824]

40. Sandelin A, Alkema W, Engstrom P, Wasserman WW, Lenhard B. JASPAR: an open-access database for eukaryotic transcription factor binding profiles. Nucleic acids research. 2004; 32:D91–94. DOI: 10.1093/nar/gkh012 [PubMed: 14681366]

41. de Laat W, Dekker J. 3C-based technologies to study the shape of the genome. Methods. 2012; 58:189–191. DOI: 10.1016/j.ymeth.2012.11.005 [PubMed: 23199640]

42. Hagege H, et al. Quantitative analysis of chromosome conformation capture assays (3C-qPCR). Nature protocols. 2007; 2:1722–1733. DOI: 10.1038/nprot.2007.243 [PubMed: 17641637]

43. Cong L, et al. Multiplex genome engineering using CRISPR/Cas systems. Science. 2013; 339:819–823. DOI: 10.1126/science.1231143 [PubMed: 23287718]

44. Cahoy JD, et al. A transcriptome database for astrocytes, neurons, and oligodendrocytes: a new resource for understanding brain development and function. The Journal of neuroscience: the official journal of the Society for Neuroscience. 2008; 28:264–278. DOI: 10.1523/JNEUROSCI.4178-07.2008 [PubMed: 18171944]

Author Manuscript Author Manuscript Author Manuscript Author Manuscript

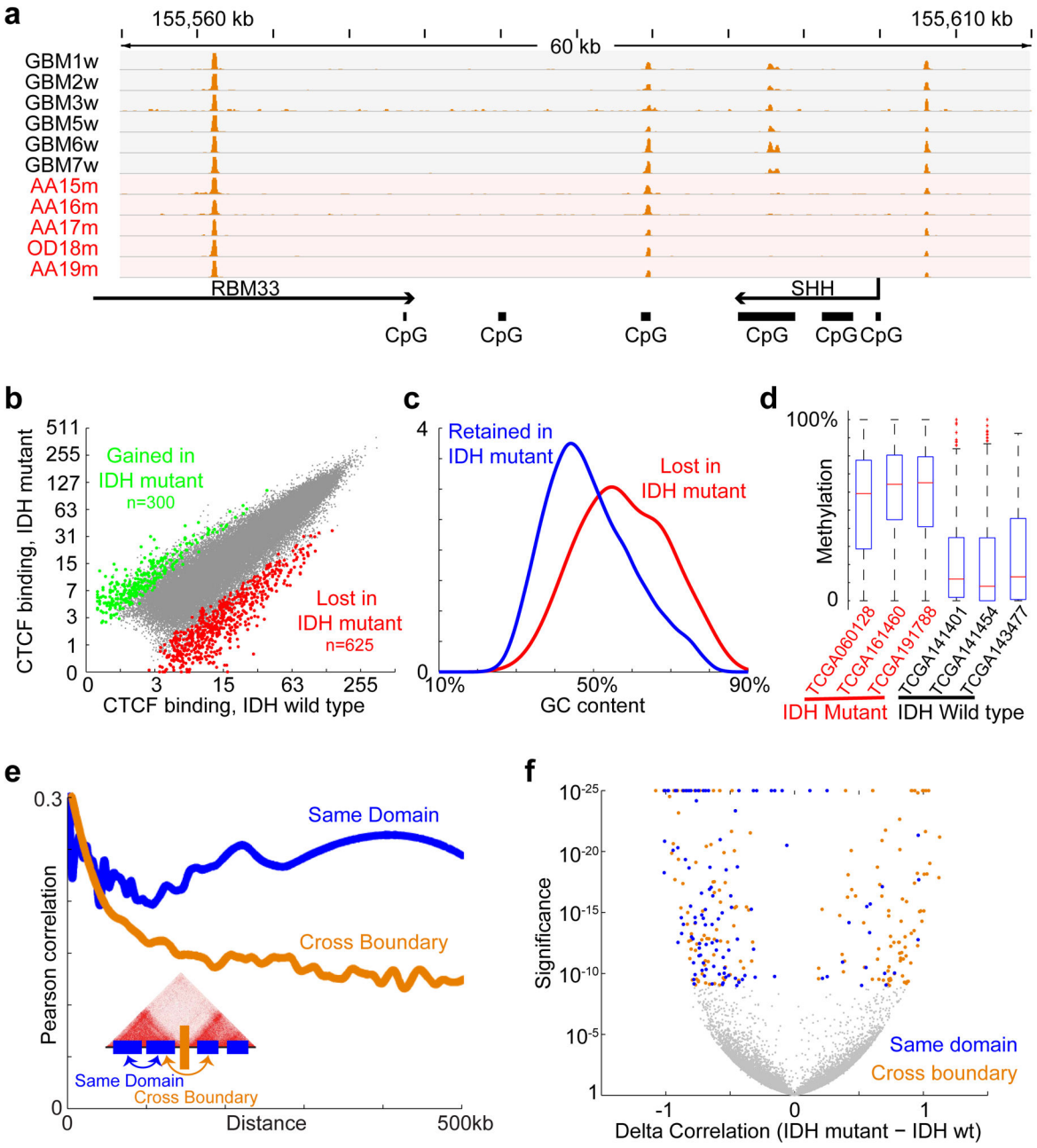

Figure 1. CTCF binding and gene insulation compromised in *IDH* mutant gliomas

(**a**) Binding profiles for the methylation-sensitive insulator CTCF are shown for a representative locus in *IDH1* mutant and wildtype tumors, normalized by average signal. (**b**) Scatterplot compares CTCF binding signals between *IDH* mutant (y-axis) and *IDH1* wildtype gliomas (x-axis) for all detected CTCF sites. A larger fraction of sites is commonly lost in all *IDH1* mutants (n=625) than gained (n=300). (**c**) Histogram compares GC content between CTCF sites that are lost or retained. (**d**) Box plots show DNA methylation levels over lost CTCF sites, as determined from whole genome bisulfite data for three *IDH* wildtype and three *IDH* mutant tumors. **(e)** Plot depicts average correlation between gene

Author Manuscript Author Manuscript Author Manuscript Author Manuscript

pairs as a function of distance across RNA-seq profiles for human brain[20]. Gene pairs separated by a constitutive CTCF-bound boundary per HiC[15] have lower correlations. (**f**) Volcano plot depicts the significance (y-axis) of gene pairs that are more (or less) correlated in *IDH* mutant than *IDH* wildtype lower-grade gliomas. Gene pairs with significantly increased correlations in *IDH* mutants (right) tend to cross boundaries (orange), while those with decreased correlations (left) more likely reside in the same domain (blue). These data indicate that *IDH* mutant, G-CIMP gliomas have reduced CTCF binding and altered expression patterns suggestive of defective gene insulation.

Author Manuscript Author Manuscript Author Manuscript Author Manuscript

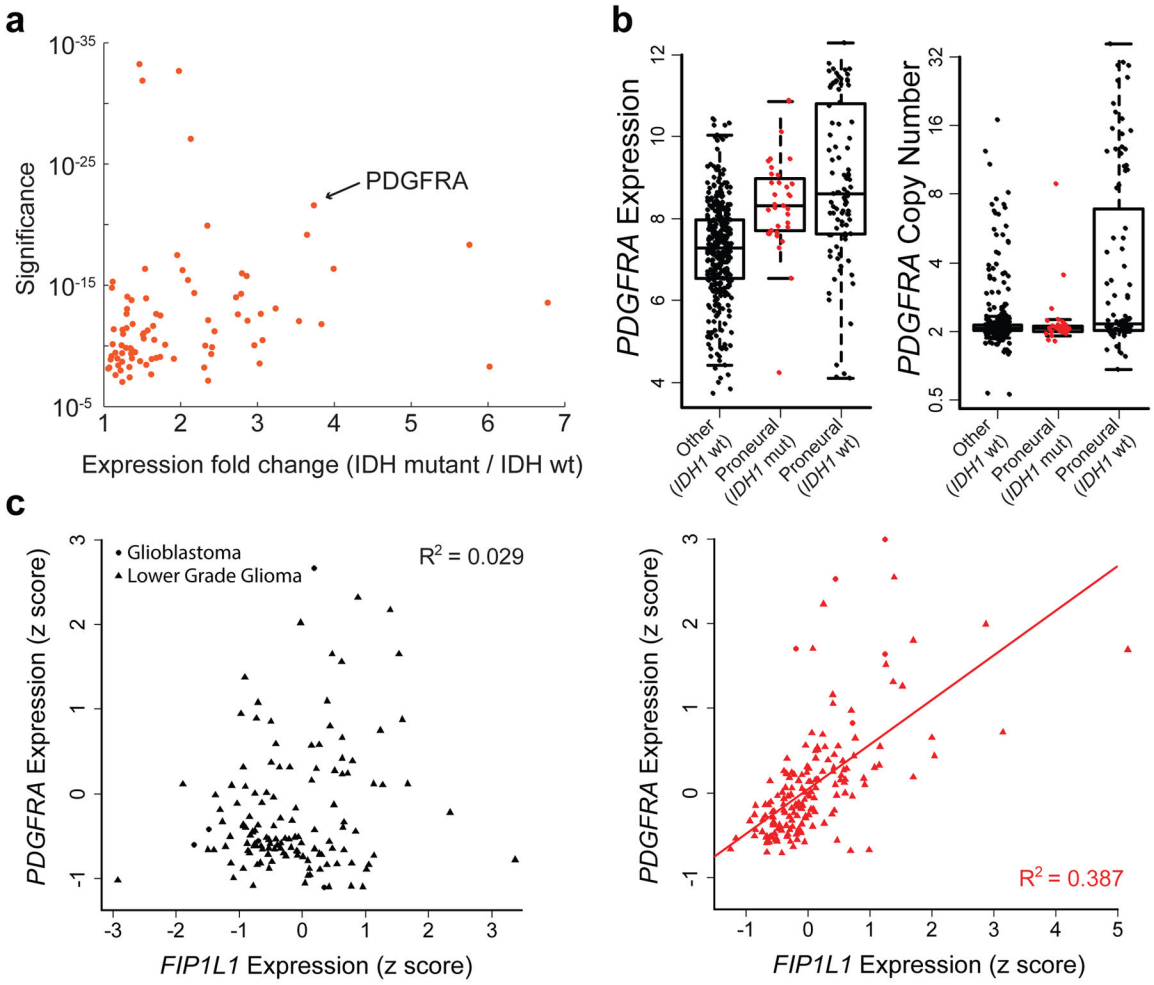

Figure 2. Topological domain boundaries disrupted in *IDH1* mutant gliomas

(**a**) Scatterplot depicts significance of deregulated boundaries in *IDH* mutant tumors (y-axis) against fold-change of most up-regulated gene in adjacent domains (x-axis). *PDGFRA* is adjacent to a significantly deregulated boundary and up-regulated in *IDH* mutants. (**b**) Boxplots compare *PDGFRA* expression (left) or copy number (right) for 443 glioblastoma tumors, classified by *IDH* status and expression subtype[24]. *IDH* mutants (red) have elevated *PDGFRA* expression, despite normal copy number. (**c**) Plots compare *PDGFRA* (y-axis) and *FIP1L1* (x-axis) expression in *IDH* wildtype (left) and mutant (right) gliomas. The genes correlate specifically in *IDH* mutants, consistent with deregulation of the intervening boundary/insulator.

Author Manuscript Author Manuscript Author Manuscript Author Manuscript

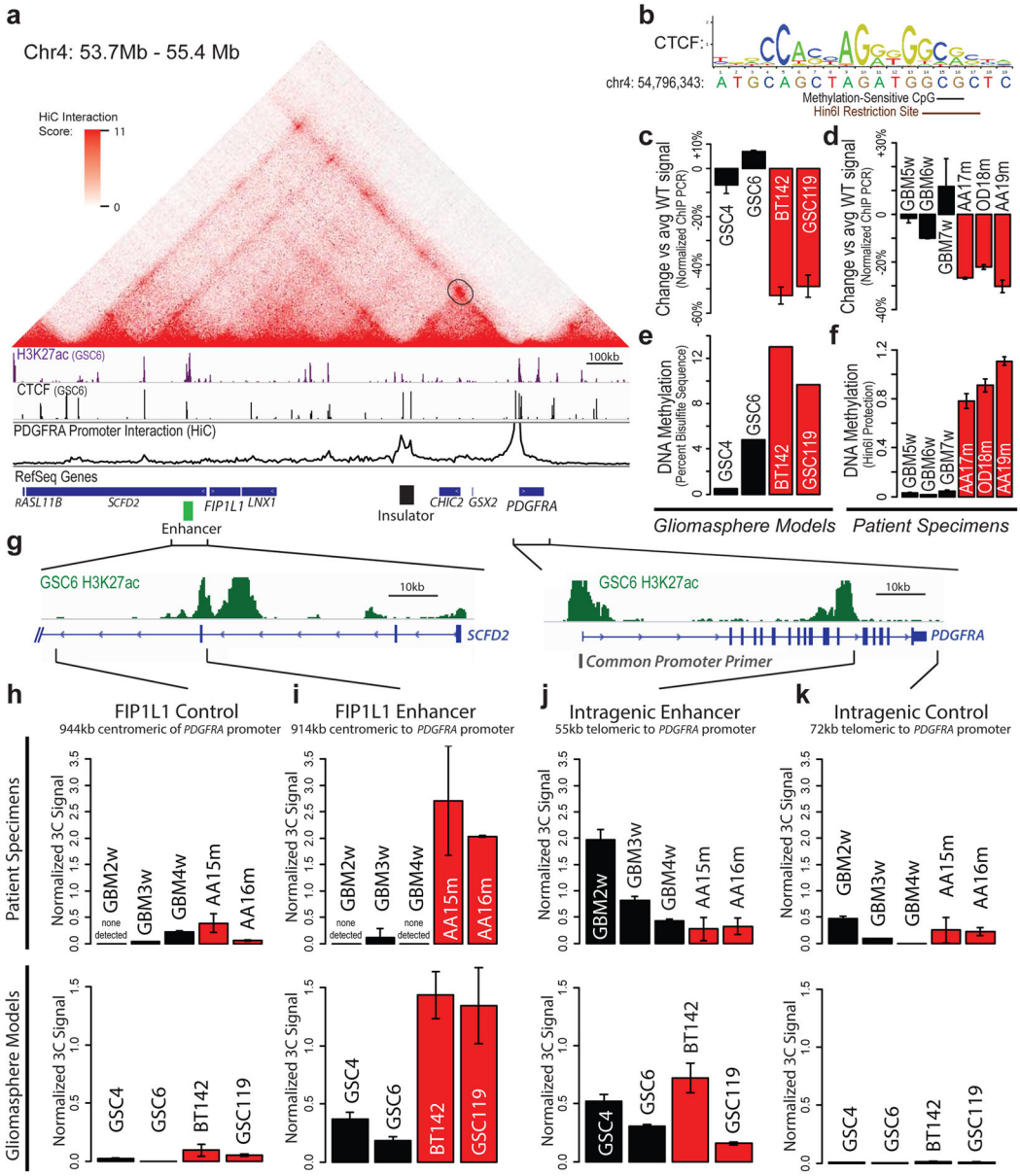

Figure 3. Insulator loss allows *PDGFRA* to interact with a constitutive enhancer

(**a**) Contact domain structure shown for a 1.7 MB region containing *PDGFRA*. Heat depicts HiC interaction scores between triangulated loci in IMR90 cells[15]. Domains are visible as triangle-shaped regions of high interaction scores. Convergent CTCF sites anchor a loop that separates *PDGFRA* and *FIP1L* (black circle). H3K27ac and CTCF profiles are aligned to the contact map. Interaction trace (below) depicts HiC signals between the *PDGFRA* promoter and all other positions in the region. Genes, *FIP1L1* enhancer (per H3K27ac) and insulator (per HiC and CTCF binding) are indicated. (**b**) The right CTCF peak in the insulator contains a CTCF motif with a CpG at a methylation-sensitive position. (**c,d**) ChIP-qPCR data show that CTCF occupancy over the boundary is reduced in *IDH* mutant (red) gliomas and models, relative to wildtype (black). (**e**) Methylation levels of the CpG in the CTCF

Author Manuscript Author Manuscript Author Manuscript Author Manuscript

motif were measured in gliomaspheres by bisulfite sequencing, and plotted as percent of alleles protected from conversion. (**f**) Methylation levels of the CpG in the CTCF motif were measured in glioma specimens by methylation-sensitive restriction, and plotted as relative protection. (**g**) Expanded views of *FIP1L1* enhancer locus and *PDGFRA* locus shown with H3K27ac tracks. Vertical black bars indicate the locations of the common *PDGFRA* promoter primer and four complementary primers tested in 3C. (**h–k**) Plots show normalized 3C interaction frequencies between *PDGFRA* promoter and indicated regions. A strong interaction between *PDGFRA* promoter and *FIP1L1* enhancer is evident in *IDH* mutant tumors and models. (Error bars in all panels reflect standard deviations of triplicate observations).

Author Manuscript Author Manuscript Author Manuscript Author Manuscript

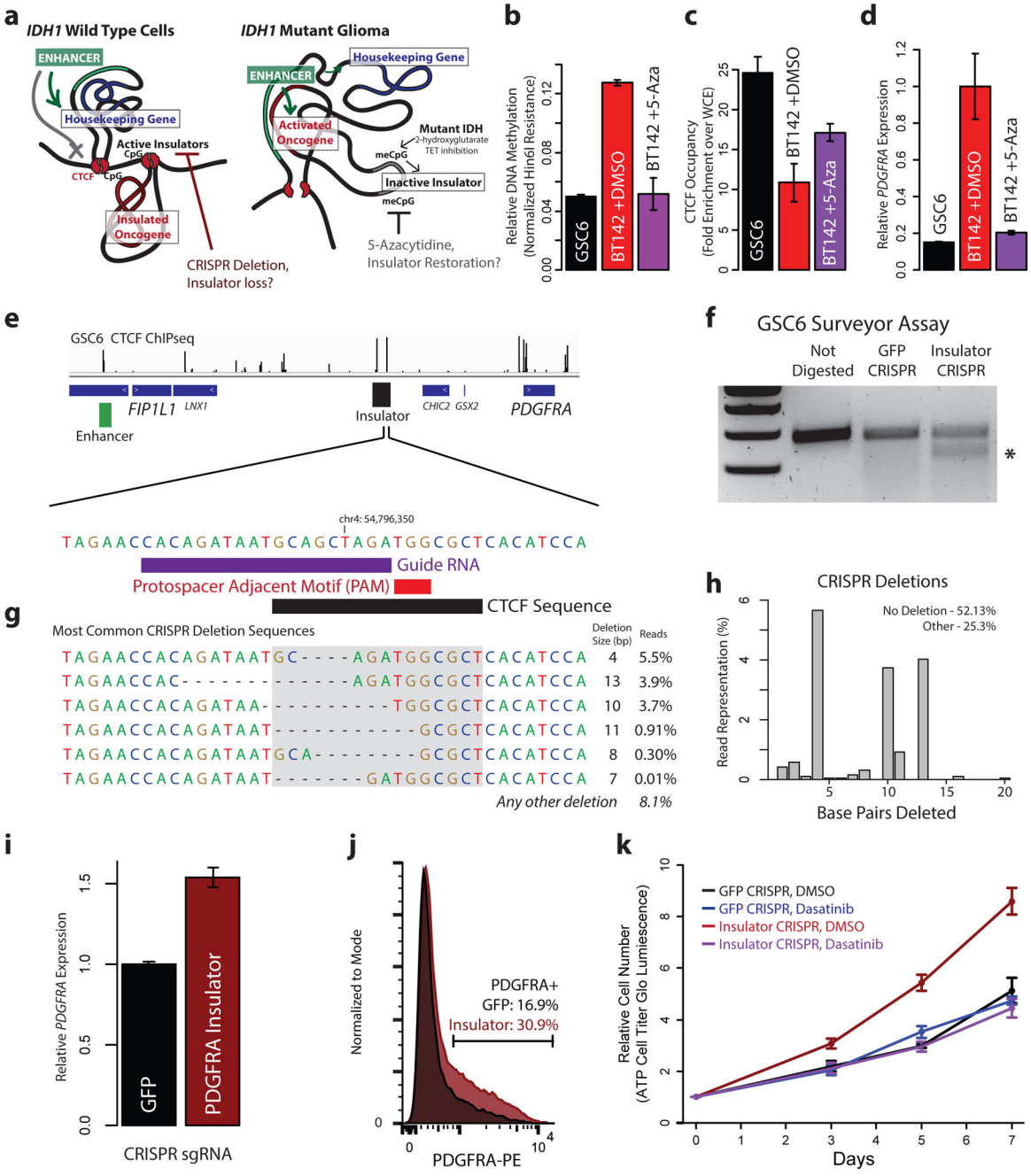

Figure 4. Boundary methylation and CTCF occupancy affect *PDGFRA* expression and proliferation

(**a**) Schematic depicts chromatin loops and boundaries in the *PDGFRA* locus. In *IDH* wildtype cells (left), intact boundary insulates oncogene. Disruption of boundary by removing CTCF motif should activate the oncogene. In *IDH* mutant (right), hyper-methylation blocks CTCF, compromising boundary and allowing enhancer to activate oncogene. Demethylation should restore CTCF-mediated insulation. (**b**) Plot compares methylation of the CpG in the CTCF motif in *IDH* wildtype gliomaspheres (black), *IDH* mutant gliomaspheres (red) and *IDH* mutant gliomaspheres treated with 5μM 5-aza for 8

Author Manuscript Author Manuscript Author Manuscript Author Manuscript

days (purple). (**c**) Plot compares CTCF occupancy over the boundary. (**d**) Plot compares *PDGFRA* expression. Demethylation restores *PDGFRA* insulation in *IDH* mutant gliomaspheres. (**e**) CTCF binding shown for the *FIP1L1/PDGFRA* region. Expanded view shows CTCF motif in the insulator targeted for CRISPR-based deletion. gRNA and protospacer adjacent motif (PAM) direct Cas9 nuclease to the motif. (**f**) Surveyor assay detects target site alterations in GSC6 gliomaspheres infected with Cas9 and sgRNA (but not in control cells infected with GFP-targeting sgRNA). (**g**) Sequencing of target site reveals the indicated deletions. CTCF motif disrupted on ~25% of alleles (compare to <0.01% in control). (**h**) Plot depicts fraction of reads in insulator CRISPR cells with a deletion of indicated size. (**i**) qPCR reveals increased *PDGFRA* expression in insulator CRISPR cells. (**j**) Flow cytometry reveals ~2-fold greater PDGFRa in insulator CRISPR cells. (**k**) Plot depicts gliomasphere growth. Insulator CRISPR cells exhibit ~2-fold increased proliferation, relative to control. This proliferation advantage is eliminated by PDGFRa inhibition. These results indicate that genetic or epigenetic disruption of the boundary compromises insulation of this oncogene. (Error bars in all panels reflect standard deviations of triplicate observations).